Reticulocyte Infection Leads to Altered Behaviour, Drug Sensitivity and Host Cell Remodelling by *Plasmodium falciparum*.

Renugah Naidu[1], Trang TT Chu[1], Jaishree Tripathi[2], Yang Hu[1], Gowtham Subramanian[1], Jie Xin Tong[3], Pallavi Tripathi[1], Kong Fang[2], Kevin SW Tan[3], Chwee Teck Lim[4], Jerry K.Y. Chan[5,6] , Zbynek Bozdech[2] and Rajesh Chandramohanadas[1*]

[1] Pillar of Engineering Product Development (EPD), Singapore University of Technology & Design (SUTD), Singapore , 487372, Singapore.

[2] School of Biological Sciences, Nanyang Technological University, Singapore

[3] Department of Microbiology and Immunology, National University of Singapore

[4] Department of Bioengineering, National University of Singapore

[5] Department of Reproductive Medicine, KK Women's and Children's Hospital, Singapore, 229899, Singapore.

[6] Duke-NUS Medical School, Singapore, 169857, Singapore.

[*] Corresponding Author: Rajesh Chandramohanadas Email: rajesh@sutd.edu.sg

Abstract

Plasmodia are host-specific, both at the organism and cellular levels. During asexual development, *Plasmodium spp.* infect cells of erythroid lineage, with an overall propensity towards reticulocytes. This applies to even *Plasmodium (P.) falciparum*, the most common causative agent of human malaria, implications of which remain unexplored. Herein, for the first time, we characterize the developmental stages and features of *P. falciparum* cultured *in vitro* in young reticulocytes ($CD71^+$) in comparison to standard normocyte ($CD71^-$) cultures. We demonstrate that there are notable differences in the patterns of invasion, development and sensitivity to potent antimalarials (such as artemisinin and dihydroartemisinin) for parasites residing in $CD71^+$ reticulocytes. Through a transcriptomic approach, we report that *P. falciparum* parasites are able to sense the host cell environment, and calibrate their metabolic and host cell remodelling pathways through differential gene expression. These results form an exciting avenue on which hitherto unexplored interactions between *Plasmodium spp* and different stages of host red blood cells could be investigated in the broader contexts of drug resistance, host tropism and zoonosis.

Author Summary

Parasites causing malaria infect red blood cells for development and proliferation during asexual development. This asexual erythrocytic stage determines higher parasite densities and eventual disease manifestation. Although the most virulent species of Plasmodium infecting humans known as *Plasmodium falciparum* is able to infect red blood cells of all ages, these parasites show a preference for younger blood cells. Of note, the biochemical and biophysical properties of young and adult red blood cells vary significantly. Herein, we undertook a comparative profiling of invasion process, parasite development and drug response of *Plasmoddium falciparum* in two host cells: young red blood cells (reticulocytes) and mature red blood cells (normocytes). We demonstrate that *P. falciparum* infects human reticulocytes with higher affinity and demonstrate differential

sensitivity to drugs such as artemisinin while they reside within reticulocytes. Furthermore, we show that *P. falciparum* is able to detect differences in host environment and adapt to it by changing the expression of genes required for host cell remodelling.

Introduction

Plasmodium infection and associated mortality remain an important concern to the developing world with 218 million malaria cases and ~450,000 deaths annually[1] (https://www.who.int/malaria/publications/world- malaria- report-2018/en/). Widespread drug-resistance [2-3] and evolution of newer phenotypes; influenced by factors such as changing availability and distribution of insect vector[4], haematological malignancies(1, 2)[5-6] (thalassemia, sickle cell anaemia, G6PD deficiency etc), providing protective immunity to certain populations[7], adversely impact malaria eradication campaigns. Furthermore, zoonotic infections from non-human primates, as in the case of *P. knowlesi*, is widely reported across Southeast Asia[8] indicating a spectrum of obscured disease manifestations challenging the developing world.

Plasmodium spp. demonstrate an overall propensity towards immature reticulocytes for asexual development. This is evident from invasion preference of rodent parasites such as *P. berghei*, known to infect reticulocytes with ~150-fold higher efficiency[9]. *P. falciparum,* which is responsible for the most severe form of human malaria, is able to infect red blood cells (RBCs) of all ages, yet with a preference to younger RBCs and reticulocytes [10]. In contrast, *P. vivax* is restricted to a sub-population of reticulocytes marked by surface transferrin receptor[11] (CD71) and are unable to infect mature RBCs. *P. knowlesi,* while able to infect all stages of RBCs in their natural macaque hosts, switch their invasion preferences to human reticulocytes during *in vitro* adaptation[12]. Since erythrocytic development is the rate limiting step in defining parasite density,

84 transmission and disease outcome, the contribution of reticulocyte infection in parasitic
85 behaviour and adaptation remain to be investigated.
86
87 *Plasmodium spp*. have simplified metabolic capacity since they are auxotrophic for
88 purines[13], vitamins and many amino acids. However, key pathways such as glycolysis,
89 tricarboxylic acid cycle (TCA), lipid synthesis, pentose phosphate pathway, pyrimidine
90 biosynthesis and glycosylation are conserved in these organisms[14-15]. To acquire
91 nutrients, parasites establish new permeation pathways in the host cells. Furthermore,
92 *Plasmodium* parasites remodel the host cells to avoid immune and mechanical
93 clearance. Many intriguing aspects of parasite-host interactions are well studied *in vitro*
94 in the case of *P. falciparum* using mature RBCs as host cells.
95
96 Reticulocytes have vastly different biochemical composition and properties. They contain
97 organelles which are expelled during maturation, through exocytosis, autophagy and
98 rearrangement of cytoskeleton[16-18]. Reticulocytes possess mitochondria with a complete
99 complement of enzymes, including an active TCA cycle[19] and are able to utilize glucose
100 through the anaerobic Embden- Meyerhof pathway and hexose monophosphate
101 shunt(3, 4). Furthermore, remnants of the transcriptional and translational machinery
102 are also present in reticulocytes. On the contrary, normocytes retain metabolic
103 processes needed for cellular survival -such as glucose oxidation and ion mobilization
104 across electrochemical gradients to maintain native hemoglobin conformation[21]. In this
105 context, the impact of two significantly different[22] host cell microenvironments: that of
106 immature reticulocytes and mature normocytes, on *P. falciparum* development remains
107 an unexplored, yet critical aspect of parasite biology.
108
109 Using reticulocytes and normocytes as *in vitro* host cells, we performed a comparative
110 study on invasion, proliferation, drug sensitivity and host-dependent adaptations of *P.*
111 *falciparum*. Our results highlight the significant differences in sensitivity of parasites

invaded into reticulocytes, for antimalarials artemisinin and dihydroartemisinin. Through a 100-cell transcriptomics study, we report key differences in the gene expression profiles associated with metabolism, antigenic variation and host cell remodeling in parasites replicated in reticulocytes. These results form an important dataset on which further investigations could be developed pertaining to the range and dynamics of parasite-host interactions with implications in progressive drug resistance and zoonosis.

Results

CD71$^+$ reticulocytes support higher invasion of *P. falciparum*

We used umbilical cord blood (KK Women's and Children's Hospital, Singapore) for this work, since peripheral blood is not an ideal source for reticulocytes in sufficient quantities. Using a magnetic selection procedure leveraging on surface expression of CD71, we purified young reticulocytes (CD71$^+$, magnet bound-fraction) and normocytes (CD71$^-$, flow through fraction). Through sub-vital staining (**Fig. 1A**) and differential interference contrast (DIC) imaging (**Fig. 1B**), separation of the red cell sub-populations was confirmed, with an estimated 90% purity as reported in prior work[22]. Through western blotting (**Fig. 1C**) and immunofluorescence microscopy (**Fig. 1D**), robust separation of the sub-populations was validated.

We estimated the comparative invasion efficiency of *P. falciparum* into CD71$^+$ and CD71$^-$ host cells. Magnet-purified schizonts (~ 40 hpi) were introduced to both host cell types and parasitemia was determined 25 h later by counting ring-stage infections. A ~2-fold higher parasitemia (**Fig. 2A**) in CD71$^+$ cells was observed. However, the number of daughter merozoites formed were comparable irrespective of the host cell (**Fig. 2B**). Interestingly, when schizonts from CD71$^+$ cells were isolated and allowed to invade CD71$^-$ cells, invasion rates similar to the controls was observed, further indicating the normal rate of parasite multiplication in CD71$^+$ cells. Gradual CD71 loss was recorded

over 48 h (**Supplementary Fig. S1A)** for healthy reticulocytes**.** Upon infection, CD71 expression was mostly unchanged up to ~18 hpi (**Supplementary Fig. S1B and S1C)** in contrast to rapid (~ 3 hpi) maturation in *P. vivax* infection[11].

Next, we carried out invasion assays in presence of varying ratios of $CD71^+$ and $CD71^-$ host cells. With an initial seeding of 1% magnet-purified schizonts, 4% rings in 100% $CD71^-$ cells and 7.5% in 100% $CD71^+$ cells were recorded. As expected, higher invasion correlated with higher amount of reticulocytes (**Fig. 2D**), with maximum infection in 100% $CD71^+$ cells. These results suggest that despite a clear preference for reticulocytes, the selection is not entirely an active parasite-driven process but likely depends on the availability and proximity of $CD71^+$ host cells. Furthermore, we did not observe higher incidents of multiply infection in reticulocytes.

Engagement of host receptors is a key step during plasmodium invasion[35]. Prior work from our group has profiled human reticulocyte proteome which indicated marginally higher amounts of basigin on reticulocyte surface (~ 1.28-fold in comparison to mature RBCs)[22] (**Supplemental Fig. S2**). As anti-basigin antibodies were shown to inhibit *P. falciparum* invasion[36] we performed invasion inhibitory studies which revealed comparable invasion of both host cells at low antibody concentrations (**Fig. 2E**). However, at higher antibody concentrations (5-10 μg/ml reported from literature), invasion into $CD71^+$ cells was less affected. This could be due to a combination of marginally higher basigin expression and larger surface area for interactions on $CD71^+$ reticulocytes.

Hence, morphology and properties of $CD71^+$ and $CD71^-$ cells were determined using single cell holotomographic analysis[25]. These analysis confirmed distinct invaginations at various planes (indicated with white arrows) (**Fig. 3A**), differentiating both cell types. Evidently, $CD71^+$ cells were irregular in shape with higher Refractive Index (RI),

indicative of a denser cytoplasmic composition (**Fig. 3B**) consistent with previous data by Park and colleagues[25]. Furthermore, CD71$^+$ cells were significantly larger (~21%) than normocytes (**Fig. 3C**), thereby presenting larger surface area for the distribution of receptors presumably leading to easier detection and attachment by plasmodial merozoites.

P. falciparum grown in reticulocytes show distinct drug sensitivity profiles

Reticulocytes possess complex membranous composition[37] and architecture rendering increased rigidity thereby influencing membrane permeability and molecular transport[38]. Previous studies show that reticulocytes have increased cation permeability for calcium (43-fold) and sodium (6- fold)[39]. Furthermore, the increased metabolic activity of CD71$^+$ reticulocytes may influence metabolism of molecules, including antimalarial drugs. In this context, we selected a broad spectrum of antimalarials (along with E64 and heparin[40], inhibitors of egress and invasion respectively) and estimated their inhibitory potential against parasites cultured in CD71$^+$ and CD71$^-$ host cells.

Trophozoite stage parasites (24-26 hpi) (or schizonts at 40-42 hpi for E64 and heparin) grown in CD71$^+$ and CD71$^-$ host cells were incubated with the drugs, along with non-treated infected RBCs. New infections were counted in the next cycle (after 50-52 h post drug treatment) and/or post invasion (20 h after treatment), for heparin and E64, followed by IC_{50} determination[26]. We observed comparable response and IC_{50} values between parasites infected into CD71$^+$ and CD71$^-$ cells for most drugs (**Supplemental Table 1**) including chloroquine. Interestingly, heparin blocked parasite invasion into CD71$^+$ cells more efficiently (IC_{50} of 1.51 μg/ml) compared to normocytes (IC_{50} of 2.82 μg/ml), while E64 showed similar egress inhibition. In contrast, cycloheximide demonstrated remarkable killing ability against parasites in CD71$^+$ cells with an estimated IC_{50} of 8.14 while infected normocytes showed an IC_{50} of 37.9 ng/ml. Host cell environment appeared to impact sensitivity of *P. falciparum* to ART and DHA (**Fig. 4A-B**), as CD71$^+$

iRBCs coped with the drug exposure better. These changes in drug sensitivity is not influenced by the different invasion rates to host cells, as confirmed by tracking parasite response to drugs during stage transition (**Supplemental Fig. S3**). Although severe malaria in children is shown to cause reduced erythropoietic responses[41], reticulocyte compensation following anemia together with sub-lethal exposure of artemisinin of parasites within $CD71^+$ reticulocytes, may render progressive drug resistance.

Host-dependent gene expression profiles in *P. falciparum*

Plasmodium spp. rely on host RBCs for metabolic needs through the consumption of host hemoglobin, vitamins and other intermediates for synthetic pathways and energy metabolism[42-44]. In addition, a range of host cell remodeling events leading to alterations in antigen presentation[45], deformability[46] and cytoadhesive properties[47] are essential for the parasite to survive within the human host. Furthermore, parasites also co-opt host cell proteins to protect from damage, stage transition and proliferation[(6, 7)-49]. Hence, we set out to investigate how the different host cell microenvironments impact parasite behavior. Owing to scarcity of samples, we adopted a modified100-cell microarray technique[27] to study gene expression profiles.

We introduced magnet-purified parasites into $CD71^+$ and $CD71^-$ cells as described in **Scheme. 1**. Trophozoites (100 infected cells) were sorted through FACS (**Fig. 6A**) for microarray. Clearly, differential gene expression in cellular pathways associated with protein and nucleotide metabolism, virulence as well as host remodeling (**Fig. 6B**) were observed. We identified 151 genes to be differentially expressed in $CD71^+$ (cycle 1) samples such as up-regulation of translation initiation factors (PF3D7_1312400, PF3D7_0528200), tRNA ligases (PF3D7_1336900, PF3D7_0407200), pyrimidine metabolism: aspartate carbamoyltransferase (PF3D7_1344800) and orotate phosphoribosyltransferase (PF3D7_0512700). On the contrary, genes such as pantothenate transporter (PF3D7_0206200) and cysteine desulfuration protein SufE[50]

(PF3D7_0206100) involved in acetyl coenzyme A formation were significantly down-regulated in parasites infected to CD71$^+$ cells (**Fig. 6C**).

3 continuous cycles of adaptation in CD71$^+$ cells led to differential expression of 26S proteasome regulatory subunits (PF3D7_1306400, PF3D7_0312300), transcription regulation and mRNA splicing related genes, such as, putative DNA-directed RNA polymerase II (PF3D7_1304900), RNA topoisomerase III (PF3D7_1347100), transcriptional regulatory protein sir2b (PF3D7_1451400) and small nuclear ribonucleoprotein-associated protein B, putative (PF3D7_1414800). Additionally, genes involved in purine and pyrimidine metabolism, such as, ribonucleoside-diphosphate reductase small chain, putative (PF3D7_1015800), adenosine deaminase (PF3D7_1029600), aspartate carbamoyltransferase (PF3D7_1344800) and orotate phosphoribosyltransferase (PF3D7_0512700) were also upregulated in cycle 3 CD71$^+$ parasites.

Several genes linked to host cell interaction and remodeling were differentially regulated in parasites inside CD71$^+$ reticulocytes. A member of the *stevor* multigene family (PF3D7_0222800), responsible for host invasion and rosetting[51] showed reduced expression in CD71$^+$ reticulocytes. In addition, *P. falciparum* erythrocyte membrane protein 1 (*Pf*EMP1) of the *var* family showed distinct patterns with PF3D7_1255200 showing reduced expression while PF3D7_0632500 showing up-regulation in CD71$^+$ host cells. Similarly, expression of knob-associated histidine-rich protein (KAHRP) (PF3D7_0202000), a major component of adhesive knobs[52] on iRBC surface was slightly down regulated in CD71$^+$ host cells, further validated through qPCR analysis (**Fig. 6C**), suggesting altered host remodeling in parasite-infected CD71$^+$ reticulocytes.

Altered host cell remodeling in *P. falciparum* infected reticulocytes

From microarray results, further validated through qPCR analyses, it appeared that expression of STEVOR, *Pf*EMP1 and KAHRP were differentially regulated which can contribute to antigenic, deformability, and cytoadherence properties of the infected cell. This was particularly interesting since we have shown in prior work that reticulocyte membrane is significantly rigid with different composition and assembly patterns of cytoskeletal components(5). Furthermore, our results also showed that infected $CD71^+$ cells maintain their characteristics up to ~20 hpi, with no indications of rapid maturation reported in the case of *P. vivax*. To elucidate possible correlations, we measured membrane deformability properties of *P. falciparum* infected $CD71^+$ and $CD71^-$ cells. Membrane of the healthy $CD71^+$ reticulocytes were significantly rigid with an estimated membrane shear modulus of 19 pN/μm compared to normocytes (average smear modulus of 6.5 pN/μm), as reported[22-37]. *P. falciparum*-infected $CD71^+$ cells remained rigid during the progression of parasites (**Fig. 7A**) in agreement with $CD71^+$ signal for up to ~20 hpi (**Supplemental S1B-C**). These findings support that *P. falciparum* is able to sense a stiffer host cell membrane ($CD71^+$) and calibrate remodeling events by altering gene expression, particularly for members of the STEVOR and *Pf*EMP1 family that are involved in these processes.

Gene profiles also suggested down-regulation of KAHRP expression, which by forming cell surface knobs facilitates endothelial adhesion. In general agreement with the data, the cell surface images generated through Atomic Force Microscopy (AFM) indicated reduced distribution of knob structures (**Fig. 7B**) on the surface of infected $CD71^+$ reticulocytes. To further quantify these differences, we estimated KAHRP expression on infected $CD71^+$ and $CD71^-$ cells through imaging flow cytometry using an antibody against KAHRP, which confirmed reduced signal from $CD71^+$ cells infected with *P. falciparum.* We were able to measure ~20% reduction in KAHRP expression in infected $CD71^+$ cells (**Fig. 7C**).

Discussion

P. falciparum and *P. vivax* present contrasting cases in terms of distribution, disease severity[53], drug sensitivity/resistance[54] and relapse[55]. Perhaps, the most intriguing aspect that differentiates these two species is the strict restriction of *P. vivax* to immature reticulocytes[11]. Since reticulocytes are formed in the bone marrow and only found in small numbers in the peripheral circulation, higher bone marrow parasitemia were reported for *P. vivax*, despite blood examination showing no infection[56] . Within the bone marrow, these parasites remain undetected and mature rapidly into transmissive forms[57]. Interestingly, homing of *P. falciparum* gametocytes in bone marrow has also been a topic of recent investigations[58]. Positive correlation between anaemia and bone marrow hemozoin/parasites in children with severe malaria reported by Aguilar *et al*[59] and others[60], indicates that bone marrow reticulocytes remain susceptible to *P. falciparum* asexual stage development.

Reticulocyte infection is advantageous for *P. falciparum* due to the abundant resources for energy metabolism and likely protection from chemical/oxidative damage. While our results do not indicate increase in *P. falciparum* multiplication rate in reticulocytes, but they appeared to better cope with damaging effects of drugs *in vitro*. Although, apparent differences in the membrane permeability and likely metabolic fate for drugs in the reticulocyte cytoplasm cannot be ruled out as a contributing factor. While RBC damage and resultant anaemia ensues over production of reticulocytes, it offers *P. falciparum* an opportunity to invade reticulocytes. Reticulocytes contain higher amounts of hemoglobin [25,61], which the parasites catabolize generating hemozoin. Artemisinin and combinations thereof target hemozoin pathway and thus required in higher dozes against *P. falciparum* residing within reticulocytes. In the light of our results, contribution of host reticulocytes in progressive drug resistance warrants systematic dissection.

306

307 Energy metabolism in *Plasmodium* depends on resources available through host RBCs
308 and beyond. For example, pantothenic acid, an essential precursor for Coenzyme A is
309 scavenged from host RBCs or culture media[62], uptake of which is facilitated by
310 pantothenate transporter (PF3D7_0206200). We observed reduction in the expression of
311 this gene in *P. falciparum* infected reticulocytes. Furthermore, gene coding cysteine
312 desulfuration SufE (PF3D7_0206100), which is also linked to Coenzyme A biosynthesis
313 was down-regulated in these parasites. This is interesting since the parasites invaded
314 into reticulocytes have an overall nutrient/energy rich environment and may not be
315 required to import and utilize extracellular pantothenate. While pantothenate transporter
316 is refractory to deletion in *P. falciparum*, its role is primarily assigned to sexual
317 differentiation[63] and transmission. Down-regulation of pantothenate transporter and
318 associated proteins (for example phosphopantetheine adenylyltransferase) may indicate
319 lesser commitment for sexual stage transition having sensed a rich environment for
320 asexual proliferation. However, this hypothesis remains to be further developed.

321

322 Cytoskeletal rearrangements leading to actin remodelling through exported proteins such
323 as *Pf*EMP1, RESA[64] and STEVOR[65] is a hallmark of *P. falciparum* asexual development.
324 KAHRP plays a critical role in iRBC rigidification through the formation of knobs[66],
325 accounting for 50% of the increased shear modulus. These changes are essential for
326 parasites that are in the peripheral circulation to avoid both immune and mechanical
327 clearance. Although *in vitro* culture conditions are known to affect transcriptional
328 profiles[67], our observations that several members of these gene families are differentially
329 regulated implies that the parasites are able to detect a vastly different host cell
330 properties, and adapt to it by changing gene expression. Afterall, if the primary location
331 of infection remains the bone marrow where reticulocytes are abundant, parasites are
332 not threatened by splenic clearance. Furthermore, *P. vivax* restricted to reticulocytes do
333 not form knobs[68] and completely lack homologs of *var* genes, offers additional premises

to undertake these observations for future research. Evolution of new biological tools such as the ability to engineer and cultivate homogeneous populations of young red blood cells for functional dissection of host factors[69-70] critical for parasite invasion, development and adaptations may contribute to such efforts.

Materials and Methods

Ethics Statement

All plasmodium experiments were conducted with approved protocols from the Institutional Biosafety Committee (IBC) of the Singapore University of Technology and Design (SUTD). Blood for routine parasite culturing and maintenance was purchased from Interstate blood bank, USA. Cord blood samples from adult normal term pregnancies were collected at KK Women's and Children's hospital with written informed consent. Protocol to collect and use cord blood for experiments was approved by the SingHealth centralised institutional Review Board (CIRB). All cord blood samples were anonymized.

Parasite culturing, synchronization and analysis

Blood was centrifuged at 600 × g for 10 min to remove buffy coat and stored in Malaria Culture Medium (MCM). Washed cord blood was incubated with CD71 magnetic microbeads for isolation of reticulocytes ($CD71^+$) through MACS (Miltenyi Biotec, Singapore), as mentioned previously(5). Unbound fraction was stored at 4°C as a source of normocytes ($CD71^-$).

3D7 strain of *P. falciparum* was used for all experiments. Parasites were maintained in 2.5% hematocrit in RPMI-HEPES medium at pH 7.4 supplemented with hypoxanthine 50 μg mL^{-1}, $NaHCO_3$ 25 mM, gentamicin 2.5 μg mL^{-1}, and Albumax II (Gibco) 0.5% wt/vol.

Schizonts (~ 45 hpi) were enriched using MACS (Miltenyi Biotech, Germany) followed by selection of rings by 5% sorbitol [23].

Blood smears prepared on glass slides were fixed with 100% methanol (Merck) and stained with fresh 1:10 Giemsa (Merck) solution. Smears from infected $CD71^+$ samples were stained with new methylene blue and examined under 100X oil immersion objective (Leica ICC50 W). Images of parasitic phenotypes were captured using a Leica digital camera[24].

Optical diffraction measurements using Tomocube™

Freshly collected RBC/reticulocyte samples were diluted 1:1000 with PBS/BSA (1%) for 2D Optical Diffraction Tomography (ODT) measurements. Images were acquired at multiple illumination angles using a 3D RI tomogram at an excitation at 532 nm (HT-2H, Tomocube, Inc., Daejeon, Korea), as described previously[25] and processed using Image J.

Antimalarial drug assays

Drugs were aliquoted at 10 mg/ml either in H_2O (chloroquine, cycloheximide, E64 and heparin), ethanol (halofantrine) or DMSO (Dihydroartemisinin, artemisinin, atovaquone, piperaquine and trichostatin A. Schizonts (~44 hpi) were introduced to $CD71^+$ and $CD71^-$ host cells separately, as seed cultures. Parasites were checked when they became trophozoites/schizonts (after ~ 35 h) through microscopy. Schizont stage parasites (40-42hpi) from the $CD71^+$ and $CD71^-$ cells were isolated and mixed with appropriate fresh host cells at 1% parasitemia and 2.5% haematocrit together with drugs. Untreated infected RBCs were included as negative controls. After 40 h, parasitemia was estimated through manual counting. Three trained researchers counted the slides independently, data represents experiments performed in triplicates. IC_{50} values were determined using GraphPad Prism according to the recommended protocol for nonlinear regression of a

log(inhibitor)-versus-response curve[26]. An unpaired t-test was applied to ensure statistical significance.

Parasite adaptation and transcriptomics

Parasites grown in $CD71^-$ and $CD71^+$ cells (1 cycle and 3 cycles), each time purifying late stage parasites (~35 hpi) on MACS and re-introducing into fresh host cells. In the next cycle, cells were harvested (30 hpi), stained with Hoechst for 30 min followed by washing in PBS before sorting 100 infected cells using a BD FACSAria™ (BD Biosciences, Singapore) into 0.2 ml tubes containing cell lysis buffer (RNase inhibitor and BSA). Samples were stored in -80°C. For cDNA amplification, cell lysates were subjected to SMART-seq2 protocol[27] and cDNA was purified using QIAGEN PCR purification kit. Before microarray hybridization, 2 to 3 µg of cDNA was labelled with Cy5 (sample) and Cy3 (reference pool) dyes and incubated for 2 h. Labelled samples were purified using QIAGEN PCR purification kit and hybridized on *P. falciparum* intragenic DNA chip at 70°C for 18 h. Next day, hybridized chips were washed and scanned on Power Scanner (Tecan).

Quantitative real-time PCR (qPCR)

qPCR was performed on two biological replicates, one set from RNA prepared for 100-cell microarray and a second fresh set of experiments. For the latter, total RNA was extracted (PureLink RNA mini kit, Life Technologies) and cleaned up through on-column digestion with PureLink DNase (Life Technologies) and reverse transcribed using the iScript™ cDNA Synthesis kit (Bio-Rad Laboratories). Real-time PCR was performed on a CFX-96 Touch System (Bio-Rad Laboratories). The PCR reactions were set up using iTaq™ Universal SYBR Green Supermix (Bio-Rad Laboratories), programmed at 30s/ 95°C followed by (10s at 95°C, 30s at 53°C) × 40. Melting curve analysis and gel electrophoresis were performed to confirm the specificity of PCR amplicons.

Gene specific primers were designed from Primer-BLAST[28], sequences are given as **Supplemental Table- 2**. *P. falciparum Arginyl-tRNA synthetase* (PF3D7_1218600) was used as reference gene[29]. We used Pfaffl method[30] to calculate normalised relative quantity (NRQ), infected normocyte (iNorm) was considered control and infected reticulocyte was considered treatment sample. The results were from two biological replicates, each with two technical replicates.

Amplification efficiency (E) of each primer pair was calculated from $E = 10^{(-1/slope)}$. The E of all primer pairs in this study were within 1.8 - 2.0.

$\Delta Ct_{gene\ of\ interest} = Ct_{goi}$ control - Ct_{goi} treatment; $\Delta Ct_{reference} = Ct_{ref}$ control - Ct_{ref} treatment.

The normalised relative quantity was calculated as below:

NRQ = $(E_{goi})^{\Delta Ct_{goi}} / (E_{ref})^{\Delta Ct_{Ref}}$ where E_{goi} and E_{ref} are respectively the amplification efficiency of target gene and reference gene *Arginyl-tRNA synthetase*.

Measurement of KAHRP expression on infected reticulocytes by ImageStream

Infected cells (42 hpi) were collected, washed with 1xPBS and fixed with 4% paraformaldehyde and 0.0075 % glutaraldehyde for 30 min at RT. Subsequently, cells were permeabilized in 0.1 % Triton X-100 for 5 min/RT. Following a quenching step in 0.1M Glycine for 30 min/RT, blocking was done overnight at 4^{o} C in 3% BSA/PBS. Incubation with anti- KAHRP monoclonal antibody (mAb 18.2, European Malaria Reagent Repository) at 5 µg/ml in 3 % BSA was done for 1 h at RT. Samples were washed and incubated with 1:500 goat anti-mouse IgG FITC antibody (Abcam, ab6785) together with 1 µg/ml Hoechst 33342 (Sigma Aldrich) in 3% BSA for 1 h at RT. After washing, cells were re-suspended in 70 µL PBS and used for imaging.

Data was acquired with ImageStream X MkII flow cytometer (Merck, Darmstadt, Germany) at 60x magnification for high-content single-cell analysis[31]. Hoechst-positive

(Ch 01) events were gated according to fluorescence intensity and visual inspection of images confirming only parasite-infected samples were being analyzed. From this, median fluorescence intensity (MFI) of FITC/KAHRP (Ch 02) was obtained. Background FITC fluorescence was deducted from doubly- stained healthy RBCs or reticulocytes used as blank controls. Single stain controls were prepared for compensation matrix generation by IDEAS software and applied for all 3 independent experiments.

AFM imaging of infected RBC surface

AFM imaging was performed with Bruker Dimension FastScan microscope (Bruker) using super sharp silicon probes (SSS-NCHR probes, Nanosensor, Switzerland) in air tapping mode[32]. Height images were captured at a resolution of 512 samples per line for 1 μm × 1 μm areas with a scan rate of 0.5 – 1 Hz. NanoScope Analysis software (version 1.90) was used to generate images with sample height profiles. Images were smoothened using a low-pass filter based on Gaussian convolution kernel, resulting into topographical height images of sample surface.

Micropipette aspiration

A micropipette with an inner diameter of 1 ± 0.25 μm was used to aspirate the RBC membrane to estimate membrane stiffness, as described in prior work[33]. A pressure drop rate of 6 Pa/s and a total pressure drop of 100 Pa were applied to aspirate and deform each cell membrane. The aspiration was visualized on a Nikon TE2000-S microscope and processed by a Labview based software. The recorded aspiration values were manually extracted, and the shear modulus was calculated using the Hochmuth model[34].

Acknowledgements

RN acknowledges SUTD Ph.D. Scholarship awarded by Ministry of Education (MoE), Singapore. RN, HY, TTTC, PT, GS and RC acknowledges infrastructure support through SUTD-MIT International Design Centre (IDC) and funding through T1MOE1702 and

RGUOO180301 grants. Miss Faith Liew's (KK Women's and Children's hospital) assistance with blood collection and Mr Benedict Lim's (Tomocube) support with 3D RI measurements are acknowledged. JCKY received salary support from Singapore's Ministry of Health's National Medical Research Council (NMRC/CSA-SI-008-2016).

Disclosure of Conflicts of Interest

The authors have declared that no competing interests exist.

References

1. World malaria Report (2018) https://www.who.int/malaria/publications/world-malaria- report-2018/en/
2. Conrad MD, Rosenthal PJ. Antimalarial drug resistance in Africa: the calm before the storm? *Lancet Infect Dis*. 2019;19(10):e338-e351.
3. Dondorp AM, Yeung S, White L, et al. Artemisinin resistance: current status and scenarios for containment. *Nat Rev Microbiol*. 2010;8(4):272-280.
4. Bamou R, Mbakop LR, Kopya E, et al. Changes in malaria vector bionomics and transmission patterns in the equatorial forest region of Cameroon between 2000 and 2017. *Parasit Vectors*. 2018;11(1):464.
5. Glushakova S, Balaban A, McQueen PG, et al. Hemoglobinopathic erythrocytes affect the intraerythrocytic multiplication of Plasmodium falciparum in vitro. *J Infect Dis*. 2014;210(7):1100-1109.
6. Guindo A, Fairhurst RM, Doumbo OK, Wellems TE, Diallo DA. X-linked G6PD deficiency protects hemizygous males but not heterozygous females against severe malaria. *PLoS Med*. 2007;4(3):e66.
7. Holz LE, Fernandez-Ruiz D, Heath WR. Protective immunity to liver-stage malaria. *Clin Transl Immunology*. 2016;5(10):e105.

500 8. Singh B, Daneshvar C. Human infections and detection of Plasmodium knowlesi.
501 *Clin Microbiol Rev*. 2013;26(2):165-184.
502 9. Cromer D, Evans KJ, Schofield L, Davenport MP. Preferential invasion of
503 reticulocytes during late-stage Plasmodium berghei infection accounts for
504 reduced circulating reticulocyte levels. *Int J Parasitol*. 2006;36(13):1389-1397.
505 10. Pasvol G, Weatherall DJ, Wilson RJ. The increased susceptibility of young red
506 cells to invasion by the malarial parasite Plasmodium falciparum. *Br J Haematol*.
507 1980;45(2):285-295.
508 11. Malleret B, Li A, Zhang R, et al. Plasmodium vivax: restricted tropism and rapid
509 remodeling of CD71-positive reticulocytes. *Blood*. 2015;125(8):1314-1324.
510 12. Lim C, Hansen E, DeSimone TM, et al. Expansion of host cellular niche can drive
511 adaptation of a zoonotic malaria parasite to humans. *Nat Commun*. 2013;4:1638.
512 13. Booden T, Hull RW. Nucleic acid precursor synthesis by Plasmodium lophurae
513 parasitizing chicken erythrocytes. *Exp Parasitol*. 1973;34(2):220-228.
514 14. Dechamps S, Shastri S, Wengelnik K, Vial HJ. Glycerophospholipid acquisition in
515 Plasmodium - a puzzling assembly of biosynthetic pathways. *Int J Parasitol*.
516 2010;40(12):1347-1365.
517 15. Barrett MP. The pentose phosphate pathway and parasitic protozoa. *Parasitol*
518 *Today*. 1997;13(1):11-16.
519 16. Liu J, Guo X, Mohandas N, Chasis JA, An X. Membrane remodeling during
520 reticulocyte maturation. *Blood*. 2010;115(10):2021-2027.
521 17. Dzierzak E, Philipsen S. Erythropoiesis: development and differentiation. *Cold*
522 *Spring Harb Perspect Med*. 2013;3(4):a011601.
523 18. Griffiths RE, Kupzig S, Cogan N, et al. Maturing reticulocytes internalize plasma
524 membrane in glycophorin A-containing vesicles that fuse with autophagosomes
525 before exocytosis. *Blood*. 2012;119(26):6296-6306.

526 19. Srivastava A, Creek DJ, Evans KJ, et al. Host reticulocytes provide metabolic
527 reservoirs that can be exploited by malaria parasites. *PLoS Pathog*.
528 2015;11(6):e1004882.
529 20. van Wijk R, van Solinge WW. The energy-less red blood cell is lost: erythrocyte
530 enzyme abnormalities of glycolysis. *Blood*. 2005;106(13):4034-4042.
531 21. Wiback SJ, Palsson BO. Extreme pathway analysis of human red blood cell
532 metabolism. *Biophys J*. 2002;83(2):808-818.
533 22. Chu TTT, Sinha A, Malleret B, et al. Quantitative mass spectrometry of human
534 reticulocytes reveal proteome-wide modifications during maturation. *Br J*
535 *Haematol*. 2018;180(1):118-133.
536 23. Subramanian G, Babu Rajeev CP, Mohan CD, et al. Synthesis and in vitro
537 evaluation of hydrazinyl phthalazines against malaria parasite, Plasmodium
538 falciparum. *Bioorg Med Chem Lett*. 2016;26(14):3300-3306.
539 24. Subramanian G, Belekar MA, Shukla A, et al. Targeted Phenotypic Screening in
540 Plasmodium falciparum and Toxoplasma gondii Reveals Novel Modes of Action
541 of Medicines for Malaria Venture Malaria Box Molecules. *mSphere*. 2018;3(1).
542 25. Kim Y, Shim H, Kim K, Park H, Jang S, Park Y. Profiling individual human red
543 blood cells using common-path diffraction optical tomography. *Sci Rep*.
544 2014;4:6659.
545 26. Subramanian G, Sadeer A, Mukherjee K, et al. Evaluation of ferrocenyl
546 phosphines as potent antimalarials targeting the digestive vacuole function
547 of Plasmodium falciparum. *Dalton Trans*. 2019;48(3):1108-1117.
548 27. Picelli S, Faridani OR, Bjorklund AK, Winberg G, Sagasser S, Sandberg R. Full-
549 length RNA-seq from single cells using Smart-seq2. *Nat Protoc*. 2014;9(1):171-
550 181.
551 28. Ye J, Coulouris G, Zaretskaya I, Cutcutache I, Rozen S, Madden TL. Primer-
552 BLAST: a tool to design target-specific primers for polymerase chain
553 reaction. *BMC Bioinformatics*. 2012;13:134.

554 29. Rocamora F, Zhu L, Liong KY, et al. Oxidative stress and protein damage
555 responses mediate artemisinin resistance in malaria parasites. *PLoS Pathog*.
556 2018;14(3):e1006930.
557 30. Pfaffl MW. A new mathematical model for relative quantification in real-time RT-
558 PCR. *Nucleic Acids Res*. 2001;29(9):e45.
559 31. Tong JX, Chandramohanadas R, Tan KSW. High-Content Screening of the
560 Medicines for Malaria Venture Pathogen Box for Plasmodium falciparum
561 Digestive Vacuole-Disrupting Molecules Reveals Valuable Starting Points
562 for Drug Discovery. *Antimicrobial Agents and Chemotherapy*. 2018;62(3).
563 32. Shi H, Liu Z, Li A, et al. Life cycle-dependent cytoskeletal modifications in
564 Plasmodium falciparum infected erythrocytes. *PLoS One*. 2013;8(4):e61170.
565 33. Sinha A, Chu TT, Dao M, Chandramohanadas R. Single-cell evaluation of red
566 blood cell bio-mechanical and nano-structural alterations upon chemically
567 induced oxidative stress. *Sci Rep*. 2015;5:9768.
568 34. Hochmuth RM. Micropipette aspiration of living cells. *J Biomech*. 2000;33(1):15-
569 22.
570 35. Cowman AF, Tonkin CJ, Tham WH, Duraisingh MT. The Molecular Basis of
571 Erythrocyte Invasion by Malaria Parasites. *Cell Host Microbe*. 2017;22(2):232-
572 245.
573 36. Aniweh Y, Gao X, Hao P, et al. P. falciparum RH5-Basigin interaction induces
574 changes in the cytoskeleton of the host RBC. *Cell Microbiol*. 2017;19(9).
575 37. Li H, Yang J, Chu TT, et al. Cytoskeleton Remodeling Induces Membrane
576 Stiffness and Stability Changes of Maturing Reticulocytes. *Biophys J*.
577 2018;114(8):2014-2023.
578 38. Blostein R, Grafova E. Factors affecting transport changes associated with
579 reticulocyte maturation. *Biomed Biochim Acta*. 1987;46(2-3):S172-176.
580 39. Wiley JS, Shaller CC. Selective loss of calcium permeability on maturation of
581 reticulocytes. *J Clin Invest*. 1977;59(6):1113-1119.

582 40. Boyle MJ, Richards JS, Gilson PR, Chai W, Beeson JG. Interactions with heparin-
583 like molecules during erythrocyte invasion by Plasmodium falciparum
584 merozoites. *Blood*. 2010;115(22):4559-4568.
585 41. Perkins DJ, Were T, Davenport GC, Kempaiah P, Hittner JB, Ong'echa JM.
586 Severe malarial anemia: innate immunity and pathogenesis. *Int J Biol Sci*.
587 2011;7(9):1427-1442.
588 42. Goldberg DE. Complex nature of malaria parasite hemoglobin degradation
589 [corrected]. *Proc Natl Acad Sci U S A*. 2013;110(14):5283-5284.
590 43. Muller S, Kappes B. Vitamin and cofactor biosynthesis pathways in Plasmodium
591 and other apicomplexan parasites. *Trends Parasitol*. 2007;23(3):112-121.
592 44. Mizuno Y, Kawazu SI, Kano S, Watanabe N, Matsuura T, Ohtomo H. In-vitro
593 uptake of vitamin A by Plasmodium falciparum. *Ann Trop Med Parasitol*.
594 2003;97(3):237-243.
595 45. Acharya P, Garg M, Kumar P, Munjal A, Raja KD. Host-Parasite Interactions in
596 Human Malaria: Clinical Implications of Basic Research. *Front Microbiol*.
597 2017;8:889.
598 46. Zhang Y, Huang C, Kim S, et al. Multiple stiffening effects of nanoscale knobs on
599 human red blood cells infected with Plasmodium falciparum malaria parasite.
600 *Proc Natl Acad Sci U S A*. 2015;112(19):6068-6073.
601 47. Alampalli SV, Grover M, Chandran S, Tatu U, Acharya P. Proteome and
602 Structural Organization of the Knob Complex on the Surface of the
603 Plasmodium Infected Red Blood Cell. *Proteomics Clin Appl*.
604 2018;12(4):e1600177.
605 48. Koncarevic S, Rohrbach P, Deponte M, et al. The malarial parasite Plasmodium
606 falciparum imports the human protein peroxiredoxin 2 for peroxide detoxification.
607 *Proc Natl Acad Sci U S A*. 2009;106(32):13323-13328.

608 49. Chandramohanadas R, Davis PH, Beiting DP, et al. Apicomplexan parasites co-
609 opt host calpains to facilitate their escape from infected cells. *Science*.
610 2009;324(5928):794-797.
611 50. Gisselberg JE, Dellibovi-Ragheb TA, Matthews KA, Bosch G, Prigge ST. The suf
612 iron-sulfur cluster synthesis pathway is required for apicoplast maintenance in
613 malaria parasites. *PLoS Pathog*. 2013;9(9):e1003655.
614 51. Niang M, Bei AK, Madnani KG, et al. STEVOR is a Plasmodium falciparum
615 erythrocyte binding protein that mediates merozoite invasion and rosetting.
616 *Cell Host Microbe*. 2014;16(1):81-93.
617 52. Rug M, Prescott SW, Fernandez KM, Cooke BM, Cowman AF. The role of
618 KAHRP domains in knob formation and cytoadherence of P falciparum-infected
619 human erythrocytes. *Blood*. 2006;108(1):370-378.
620 53. Battle KE, Lucas TCD, Nguyen M, et al. Mapping the global endemicity and
621 clinical burden of Plasmodium vivax, 2000-17: a spatial and temporal modelling
622 study. *Lancet*. 2019;394(10195):332-343.
623 54. Haldar K, Bhattacharjee S, Safeukui I. Drug resistance in Plasmodium. *Nat Rev*
624 *Microbiol*. 2018;16(3):156-170.
625 55. Looareesuwan S, White NJ, Chittamas S, Bunnag D, Harinasuta T. High rate of
626 Plasmodium vivax relapse following treatment of falciparum malaria in Thailand.
627 *Lancet*. 1987;2(8567):1052-1055.
628 56. Rumball CA, Parsons-Smith BG, Nancekievill L. Sternal puncture in the diagnosis
629 of malaria. *Lancet*. 1943;242(6268):468–469.
630 57. Obaldia N, Meibalan E, Sa JM, et al. Bone Marrow Is a Major Parasite Reservoir
631 in Plasmodium vivax Infection. *Mbio*. 2018;9(3).
632 58. De Niz M, Meibalan E, Mejia P, et al. Plasmodium gametocytes display homing
633 and vascular transmigration in the host bone marrow. *Science Advances*.
634 2018;4(5).

635 59. Aguilar R, Moraleda C, Achtman AH, et al. Severity of anaemia is associated with
636 bone marrow haemozoin in children exposed to Plasmodium falciparum. *British*
637 *Journal of Haematology*. 2014;164(6):877-887.
638 60. Smalley ME, Abdalla S, Brown J. The Distribution of Plasmodium-Falciparum in
639 the Peripheral-Blood and Bone-Marrow of Gambian Children. *Transactions of*
640 *the Royal Society of Tropical Medicine and Hygiene*. 1981;75(1):103-105.
641 61. Rai D, Wilson AM, Moosavi L. Histology, Reticulocytes. StatPearls. Treasure
642 Island (FL); 2019.
643 62. Trager W. Coenzyme A and the antimalarial action in vitro of antipantothenate
644 against Plasmodium lophurae, P. coatneyi and P. falciparum. *Trans N Y*
645 *Acad Sci*. 1966;28(8):1094-1108.
646 63. Hart RJ, Cornillot E, Abraham A, et al. Genetic Characterization of Plasmodium
647 Putative Pantothenate Kinase Genes Reveals Their Essential Role in
648 Malaria Parasite Transmission to the Mosquito. *Sci Rep*. 2016;6:33518.
649 64. Diez-Silva M, Park Y, Huang S, et al. Pf155/RESA protein influences the dynamic
650 microcirculatory behavior of ring-stage Plasmodium falciparum infected red blood
651 cells. *Sci Rep*. 2012;2:614.
652 65. Sanyal S, Egee S, Bouyer G, et al. Plasmodium falciparum STEVOR proteins
653 impact erythrocyte mechanical properties. *Blood*. 2012;119(2):e1-8.
654 66. Glenister FK, Coppel RL, Cowman AF, Mohandas N, Cooke BM. Contribution of
655 parasite proteins to altered mechanical properties of malaria-infected red
656 blood cells. *Blood*. 2002;99(3):1060-1063.
657 67. Tilly AK, Thiede J, Metwally N, et al. Type of in vitro cultivation influences
658 cytoadhesion, knob structure, protein localization and transcriptome profile of
659 Plasmodium falciparum. *Sci Rep*. 2015;5:16766.
660 68. Totino PR, Lopes SC. Insights into the Cytoadherence Phenomenon of
661 Plasmodium vivax: The Putative Role of Phosphatidylserine. *Front Immunol*.
662 2017;8:1148.

69. Kanjee U, Gruring C, Chaand M, et al. CRISPR/Cas9 knockouts reveal genetic interaction between strain-transcendent erythrocyte determinants of Plasmodium falciparum invasion. *Proc Natl Acad Sci U S A*. 2017;114(44):E9356-E9365.

70. Satchwell TJ, Wright KE, Haydn-Smith KL, et al. Genetic manipulation of cell line derived reticulocytes enables dissection of host malaria invasion requirements. *Nat Commun*. 2019;10(1):3806.

Figure legends

Figure- 1. Purification and characterisation of CD71$^+$ and CD71$^-$ red blood cells. A. CD71$^+$ reticulocytes were purified from cord blood using Magnetic-activated cell sorting (MACS) protocol. Isolated sub-fractions were inspected through sub vital staining (Top) and differential interference microscopy (Bottom). **B.** Immunofluorescence microscopy confirmed abundant localisation of CD71 on immature reticulocytes (magnet-bound fraction). Cells were stained with Cell Mask^{TM} Red (Thermo Fisher Scientific) and α-CD71 antibody (Green). **C.** Western blotting showed robust purification of CD71$^+$ reticulocytes. Probing was performed with α-CD71 antibody (1:1000, Abcam), with GAPDH (1:1000, Abcam) serving as loading control.

Figure- 2. Comparison of *P. falciparum* infection in CD71$^+$ and CD71$^-$ blood cells. A. Approximately 2-fold higher infection of *P. falciparum* was observed when CD71$^+$ reticulocytes (purple) were used as host cells. (Mean values of 2 independent experiments; CD71$^+$: 10.52% and CD71$^-$: 5.08%). An unpaired two-tailed t-test was performed to confirm statistical reliability. **B.** Merozoite counts were taken from late stage segmented schizonts through fluorescence microscopy, which showed comparable values irrespective of the host cells used for infection (Mean values of 2 independent experiments; CD71$^-$: 24.28 and CD71$^+$: 24.80). **C.** Parasites grown in CD71+

reticulocytes for one cycle were re-introduced to CD71- cells, which showed invasion rates similar to controls, suggesting merozoite production is not increased during development inside reticulocytes. **D.** Higher amounts of reticulocytes in the culture wells resulted in increased infection rate *in vitro*. However, maximum infection was achieved only in a pure $CD71^+$ reticulocyte population. **D.** Invasion efficiency comparison in presence of varying amounts of anti-basigin antibody**,** saturating levels of the antibody showed differential effects on reticulocyte invasion while completely blocking *P. falciparum* invasion into normocytes.

Figure- 3. Holotomography measurements demonstrate that $CD71^+$ reticulocytes are larger and multi-lobular. A. Representative holotomography images of $CD71^+$ and $CD71^-$ cells demonstrating comparative cellular morphologies. Using Tomocube HT-1, we derived quantitative dynamic cell measurements on **B**. Refractive index (Mean values of 20 cells; $CD71^-$: 1.37 and $CD71^+$: 1.40) and **C**. surface area (Mean values of 20 cells; $CD71^-$: 238.00μm^2 and $CD71^+$: 267.75μm^2). These measurements revealed that $CD71^+$ reticulocytes are ~20% larger than normocytes.

Figure- 4. *P. falciparum* grown in $CD71^+$ retioculocytes show different sensitivity to artemisinin family drugs. Growth inhibition assays against 3D7 parasites infected into distinct host cell populations was conducted. Infected cells were incubated with antimalarials at the early trophozoite stage (32 to 36 hpi) and parasitemia was manually counted (5000 cells) in the next cycle of trophozoite stage. The experimental data represents the mean of 3 independent experiments performed in replicates. Figure shows the log (inhibitor)-versus-response curves for potent antimalarials on *P. falciparum* infected $CD71^+$ and $CD71^-$ cells for **A**. artemisinin, **B.** dihydroartemisinin, **C.** cycloheximide and **D.** chloroquine.

Figure- 5: Schematic representation of parasite adaptation and enrichment strategy adopted for 100- cell microarray analysis. *P. falciparum* schizonts were allowed to invade into cord blood normocytes (for 3 continuous cycles), $CD71^+$ reticulocytes (for 1 cycle) and in $CD71^+$ reticulocytes for 3 consecutive cycles. For the third condition, schizonts in every cycle was purified and re-introduced into freshly purified reticulocytes (to avoid any invasion to normocytes resulting from maturation while in culture) from the same batch of blood. After staining with Hoechst, 100-infected cells were isolated by FACS sorting and subsequent microarray analysis.

Figure- 6: Differential Gene expression profiles in *P. falciparum* adapted in human reticulocytes. Expression profiles of genes in *P. falciparum* adapted into $CD71^+$ and $CD71^-$ cells. **A.** 100 infected cells from $CD71^-$ cultures (3 cycles), and $CD71^+$ cultures (1 cycle and 3 cycle) were isolated through FACS sorting, flow plots demonstrating gating and purity of cells (top panel). Uninfected/healthy cells were used as negative control for gating (bottom). **B.** Upon completing microarray analysis, a Z-score cut-off of 2 was applied to only assess genes, which showed stable difference between the two conditions when comparing both biological replicates. List of genes which are more than 2-fold up or down-regulated when comparing $CD71^-$ host cells to $CD71^+$ reticulocytes cycle 1 or cycle 3 was obtained. This analysis gave 156 genes different between normocytes versus reticulocytes in 1 cycle and 159 genes different between $CD71^-$ versus $CD71^+$ in 3 cycles represented in the above heatmap (based on Euclidean distance) shows the expression for these differentially expressed genes in the three conditions compared. Red represents up-regulated genes, purple represents down-regulated genes and white represents no change in expression. ($CD71^-$ refers to normocytes, 3 cycles, 5 replicates; R1: refers to $CD71^+$, 1 cycle, 5 replicates; R3 refers to $CD71^+$, 3 cycles, 5 replicates). **C**. Based on microarray data, the differential expression of six selected genes were confirm by quantitative real-time PCR: *KAHRP* (PF3D7_0202000), *stevor* (PF3D7_0222800), *var* (PF3D7_0632500), *pantothenate*

745 *transporter* (PF3D7_0206200), *phosphopantetheine adenylyltransferase*
746 (PF3D7_0704700) and cysteine desulfuration SufE (PF3D7_0206100) confirming
747 microarray results. Normalised quantitative expression to *arginyl-tRNA synthetase* was
748 compared between infected $CD71^-$ (control) and infected $CD71^+$ (treatment). The graphs
749 show two data points from two independent biological experiments.
750
751 **Figure- 7: Host cell remodelling in *P. falciparum* infected reticulocytes is altered**
752 **through differential gene expression.** **A.** Membrane of *P. falciparum* infected
753 reticulocytes ($CD71^+$) remain stiff during early parasite development, as measured
754 through micropipette aspiration technique. Briefly, 30-40 cells were obtained per
755 measurement for individual experiments. The cellular membrane was monitored by
756 Olympus IX71 microscope and image was processed by QCapture Pro 6.0 and the
757 elastic shear modulus was determined using the Hochmuth model. **B.** Surface view of
758 infected $CD71^-$ and infected $CD71^+$ cells scanned by AFM showing an area of 1µm on a
759 representative cell, indicating reduced knob formation in infected $CD71^+$ reticulocytes.**C**.
760 Reduced KAHRP expression on infected $CD71^+$ cells was validated through Amnis
761 Imaging flow cytometry. Infected cells were labeled with anti-KAHRP antibody and
762 stained with secondary anti-mouse FITC antibody together with Hoechst. Background
763 FITC fluorescence was deducted from doubly-stained uninfected healthy cells: CD71-
764 and CD71+, as appropriate. Graphs shows results from three independent experiments.
765
766
767 **Supplemental Table. 1: IC_{50} values for *P. falciparum* grown under two host**
768 **conditions against selected antimalarial drugs.**
769
770 **Supplemental Table. 1: A list of genes with corresponding PCR primers used for**
771 **qPCR experiments**
772

Supplementary Figure-1. *P. falciparum*- infected red cells remain CD71$^+$ until parasites progress into late rings/early trophozoites. A. CD71$^+$ samples were stained with anti-CD71 antibody at 1:100 and secondary antibody (Alexa Fluor 488 at 1:200). Differential interference microscopy (DIC) show morphological characteristics of reticulocytes still present at ~24 h. **B.** Fluorescence intensity of stage specific depletion of CD71 on uninfected CD71$^+$ verses infected CD71$^+$ reticulocytes ('+' indicated presence of fluorescence, '-' indicated absence of fluorescence; based on 1000 infected cells). Samples were imaged on coverslips and captured at 100x oil magnification using a CKX53 Olympus microscope. **C.** Sub vital stain of cells at specific stages of infection (ring ~18 to 24 h), trophozoite (~24 to 36 h) and schizont (~ 40 to 44 h) show absence of RNA (green arrow) in infected while uninfected CD71$^+$ cells still harbour reticular matter (red arrows). (ui: uninfected ; i: infected). Bar graph depiction of the premature loss of CD71 on infected reticulocytes in comparison to uninfected reticulocytes.

Supplementary Figure-2. Surface expression of known host receptors required for *P. falciparum* invasion (Results originating from Mass spectrometry data, reported in Chu *et al*, 2018).

Supplementary Figure-3. Differential sensitivity of antimalarial drugs between infected reticulocytes and infected normocytes is not caused by differences in the invasion rates. Seeding cultures for both infected host cells were reduced to the same parasitemia of 1% followed by treatment of antimalarials **A.** artemisinin **B.** dihydroartemisinin **C.** cycloheximide and **D.** chloroquine at IC_{50} and IC_{80} concentrations at early trophozoite stage and parasitemia was manually counted in the next cycle of trophozoite stage (32 to 36 h post invasion).

Supplementary Figure- 4. Pathway enrichment results demonstrating altered metabolism and host cell remodelling in (A) parasites grown for 1 cycle in CD71^{+} reticulocytes and (B) parasites grown for 3 continuous cycles in reticulocytes.

Supplementary Figure- 5: Relative mRNA levels of interseting candidate genes across 3 cycles of host cell switching (N-R1) and adpatation (R1-R3) Genes such as **(A)** var (PF3D7_1255200), **(B)** KAHRP, **(C)** Pantothenate transporter and **(D)** orotate phosphoribosyl transferase are higlighted. Transcript levels were measure by qPCR and shown as normalised relative quantity to internal control *arginyl-tRNA synthetase* gene. Results were from one biological experiment of the RNA sample used for microarray data.

S6. Representative images of infected CD71^{+} and CD71^{-} red cells obtained from Imaging flow cytometry, demonstrating reduced fluorescence signal in infected CD71- host cells.

S7. Surface patterns of healthy (un-infected) CD71^{+} and CD71^{-} red blood cells, used as controls for studying the presence of knobs.

S8: Genes identified and fold difference from the Microarray experiments

Authorship Contributions

RN, TTTC, JT, YH, GS, JXT, PT and KF carried out laboratory work and collected and analyzed the data; JC provided clinical management of cord blood related aspects, ethical clearance, and collection and processing of the blood samples; **RN, TTTC, JT, HY, GS, JXT, PT, KF, KST, CT, JC and ZB** participated in data interpretation and helped to draft the manuscript; **RC** designed the study, coordinated the project and wrote

826 the manuscript. The funders had no role in study design, data collection and analysis,
827 decision to publish, or preparation of the manuscript.

828

829

Figure. 1

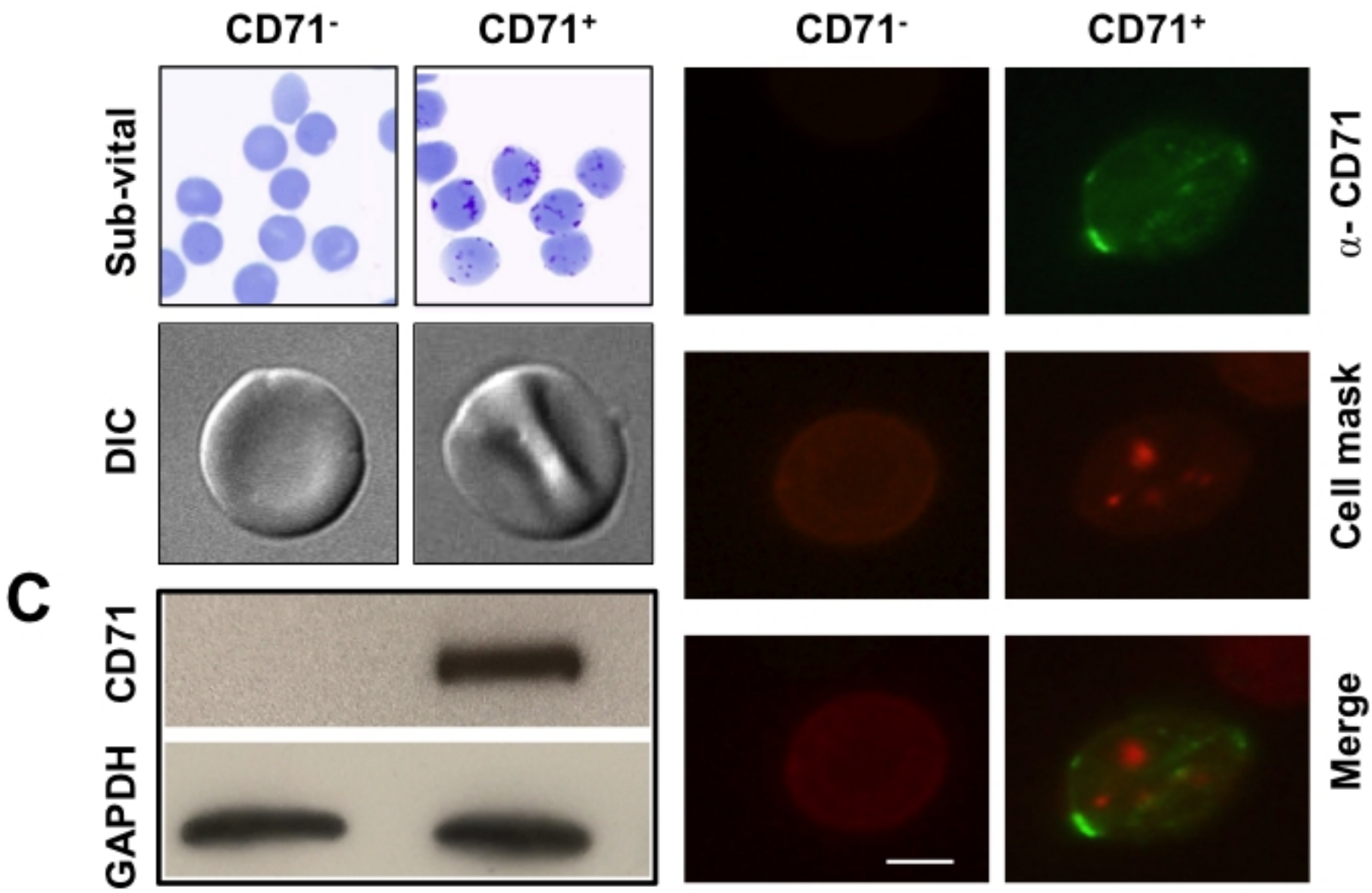

Figure. 1

Figure. 2

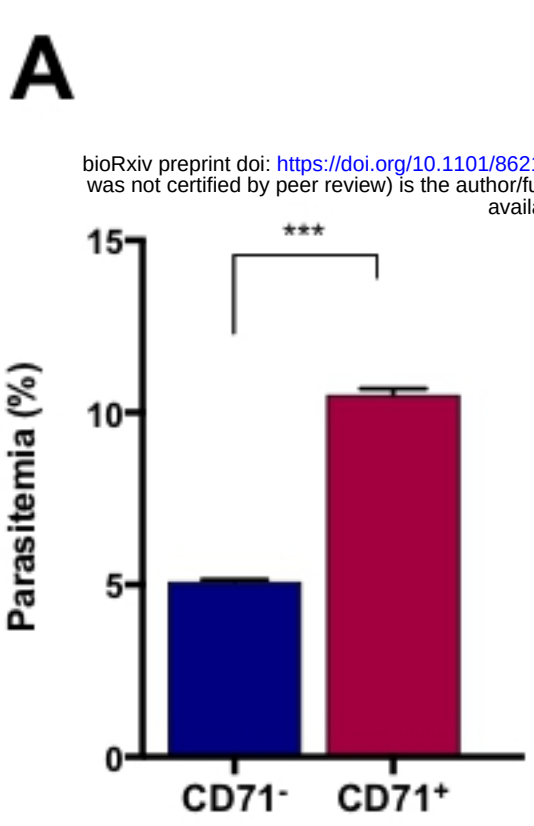

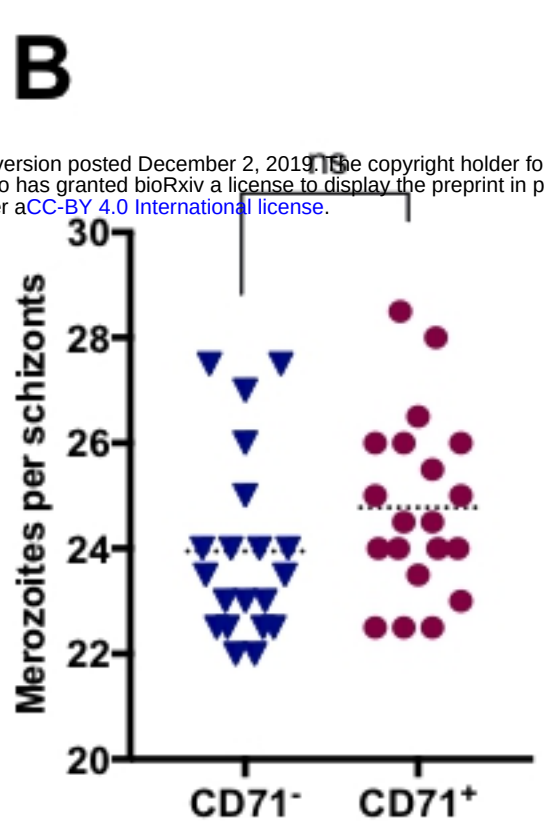

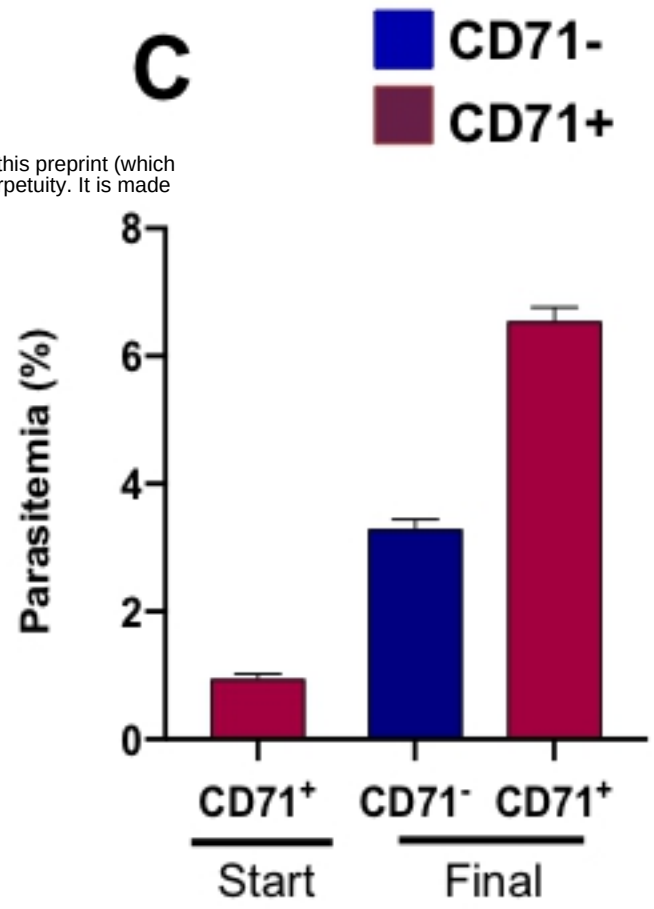

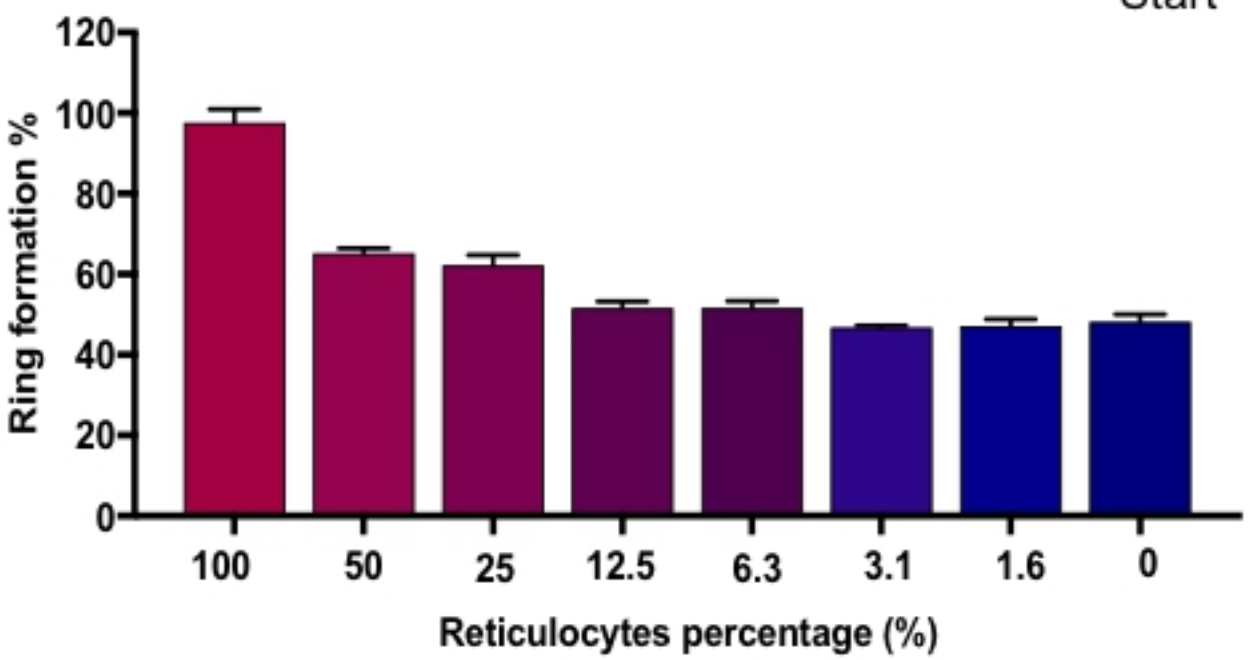

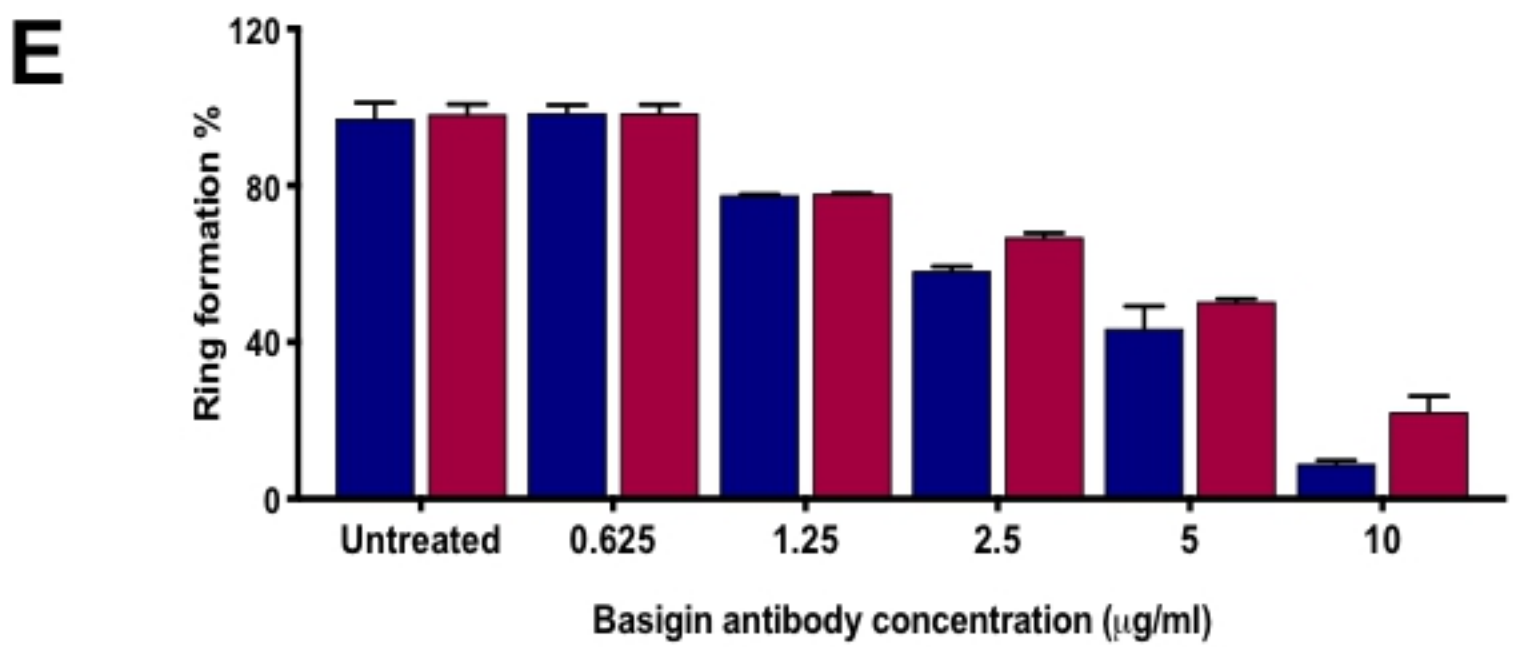

Figure. 2

Figure. 3

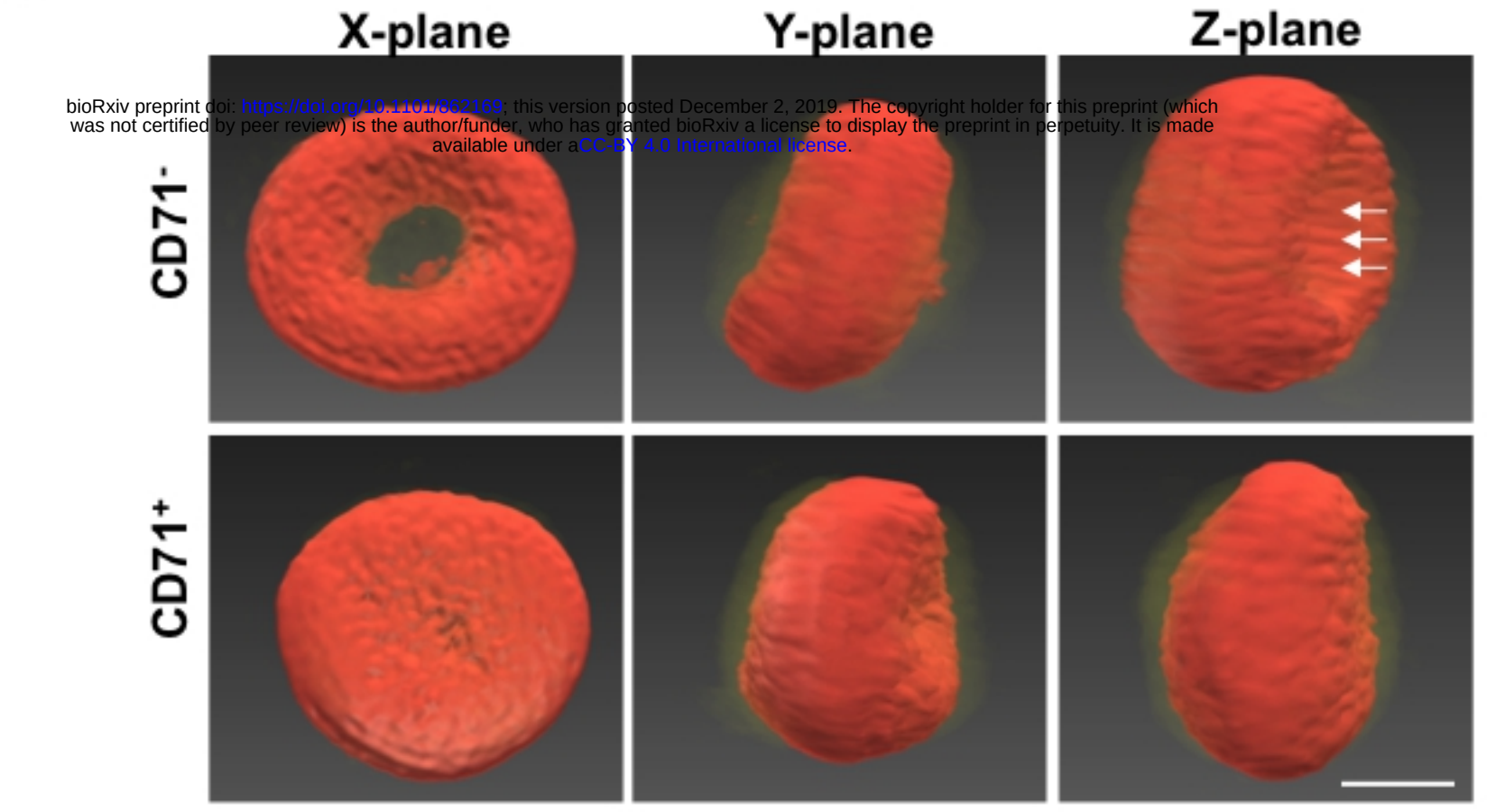

Figure. 3

Figure. 4

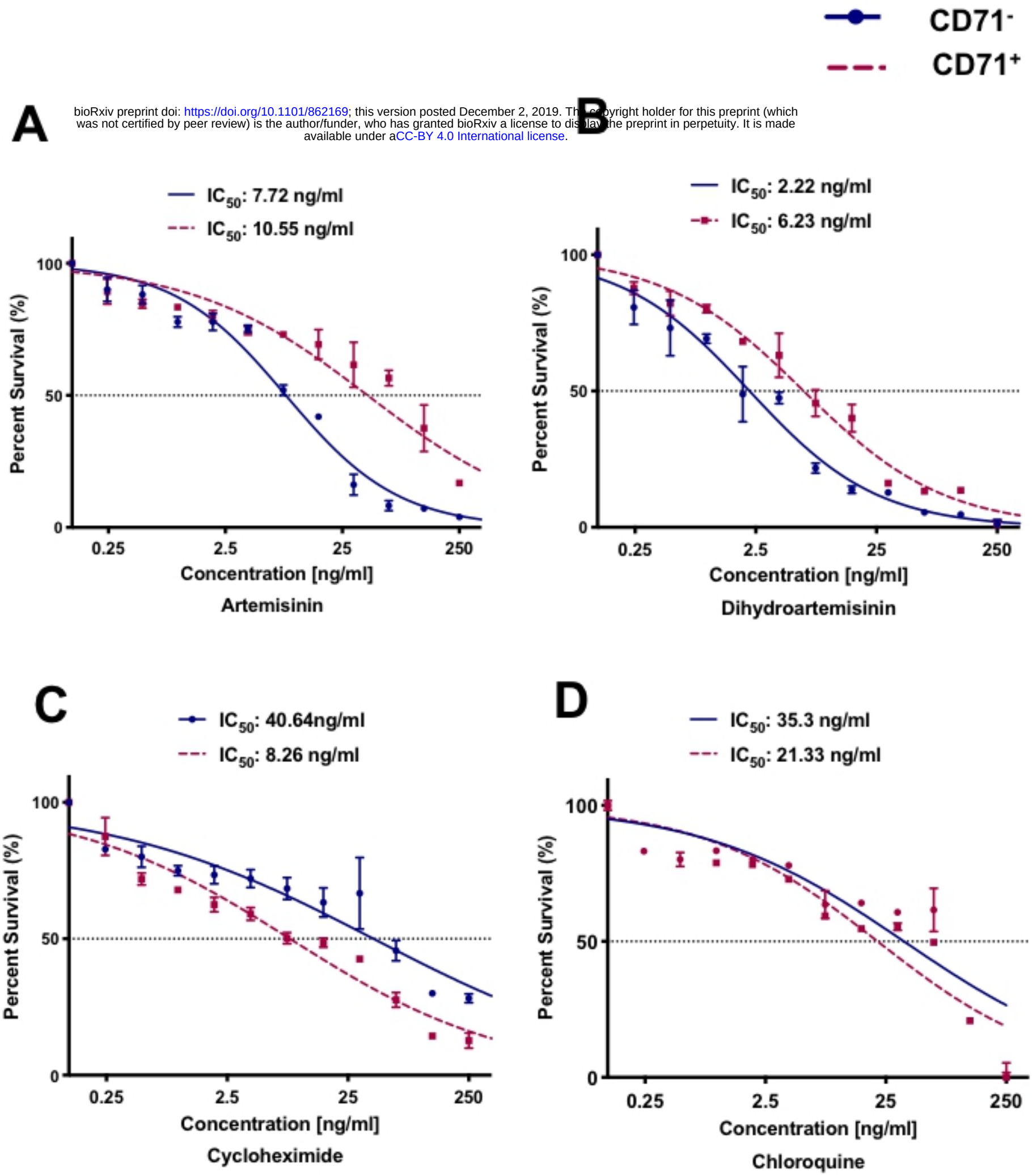

Figure. 4

Figure. 5

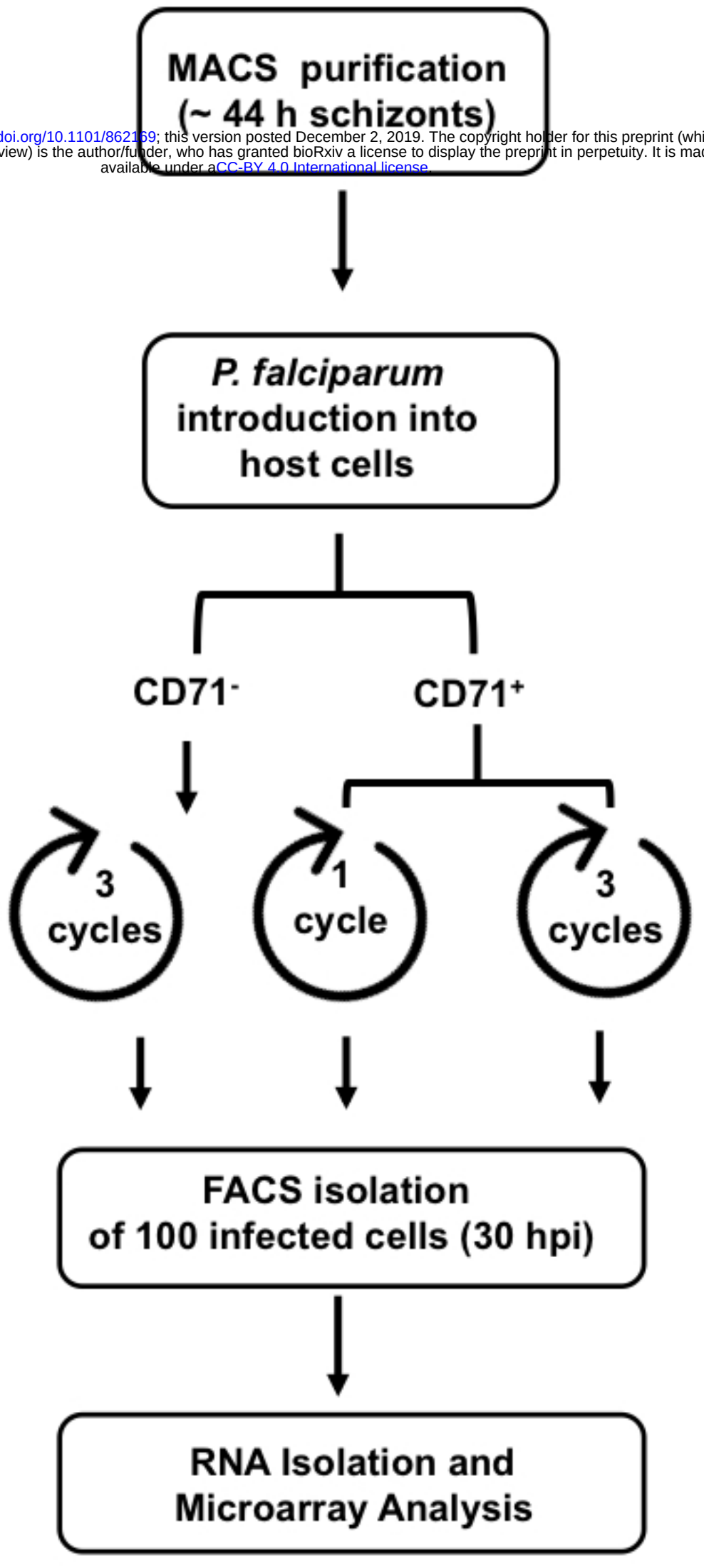

Figure. 5

Figure. 6

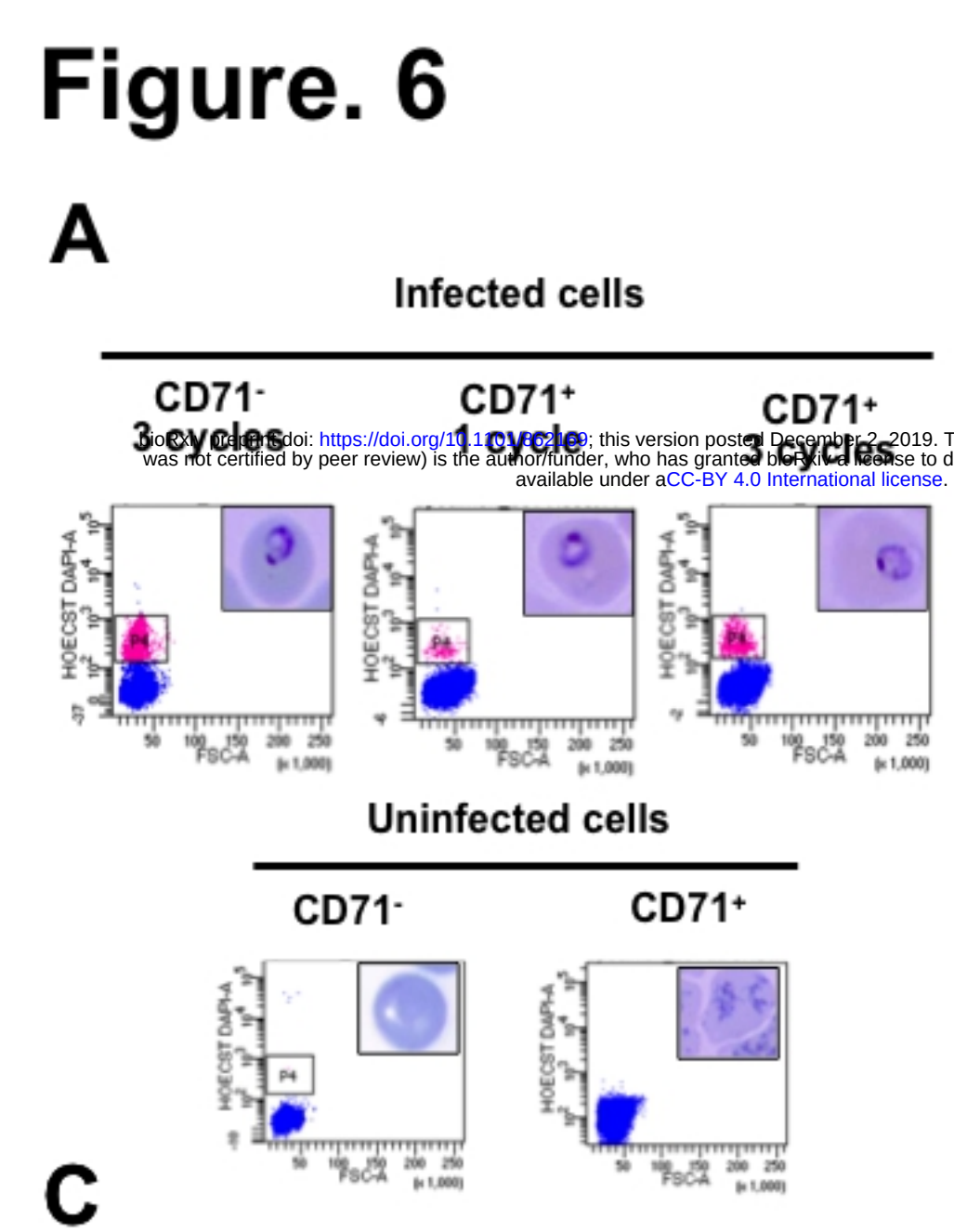

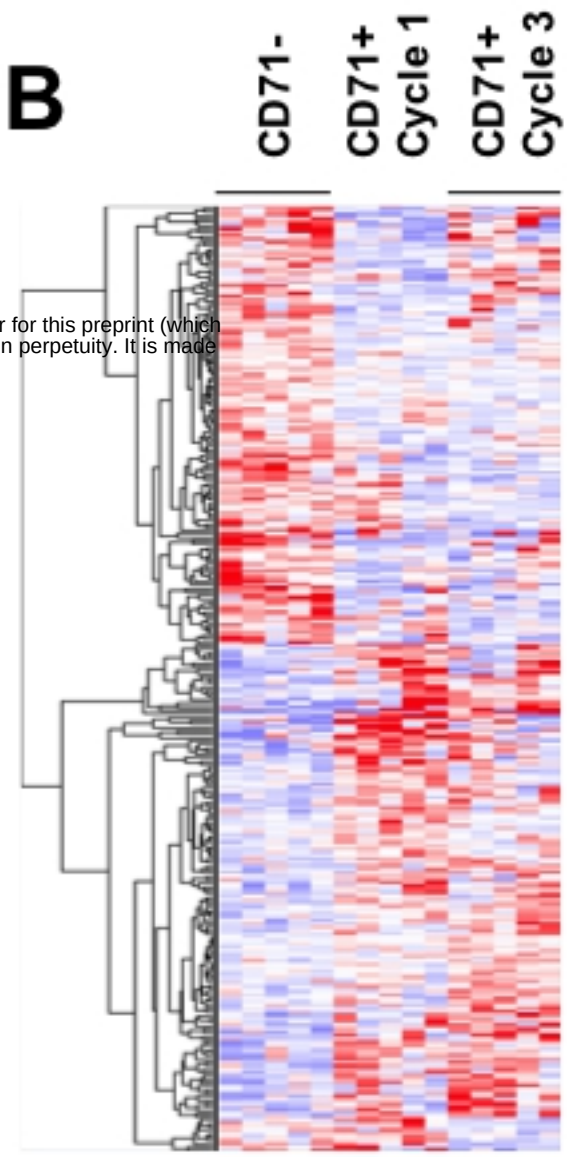

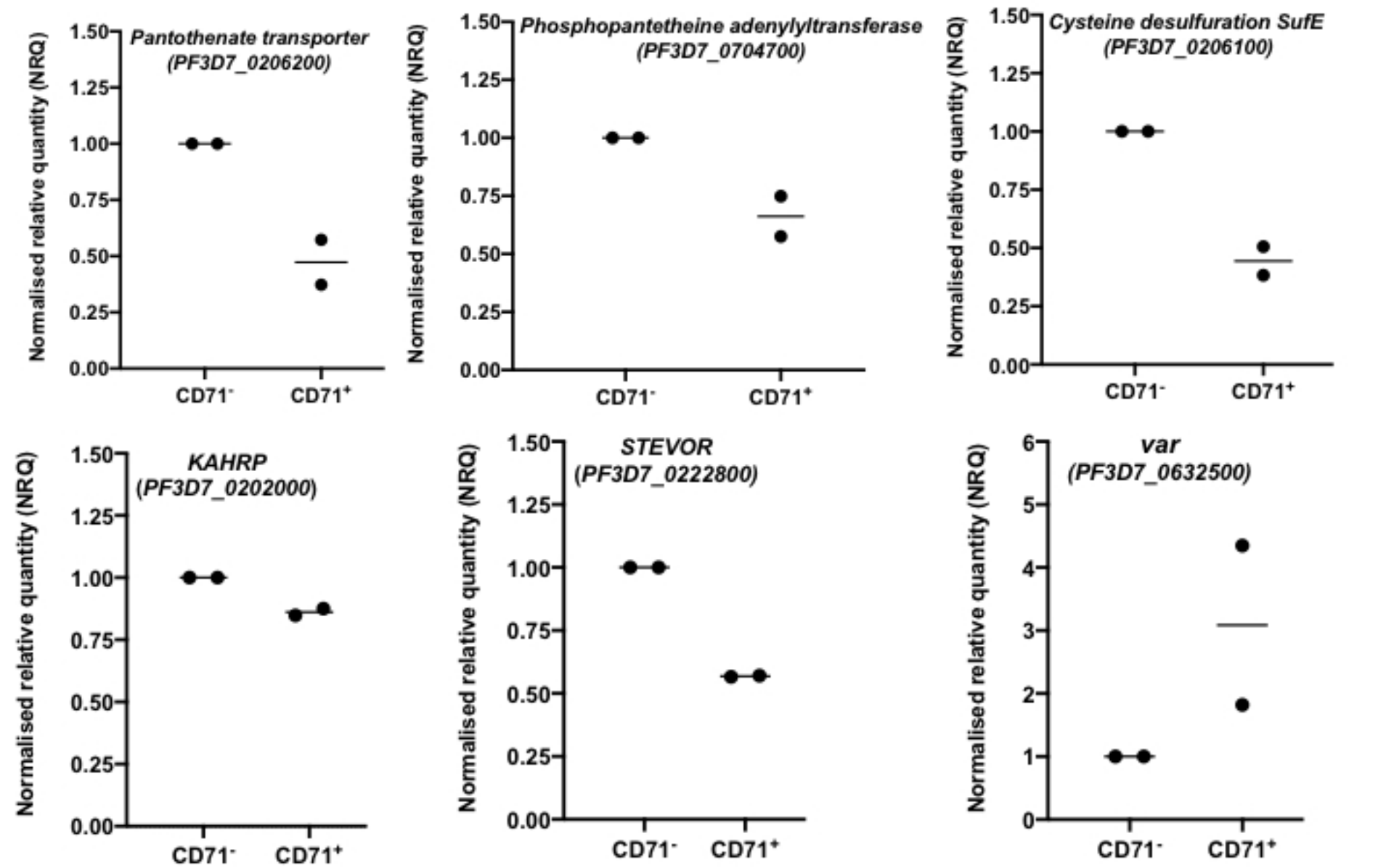

Figure. 6

Figure. 7

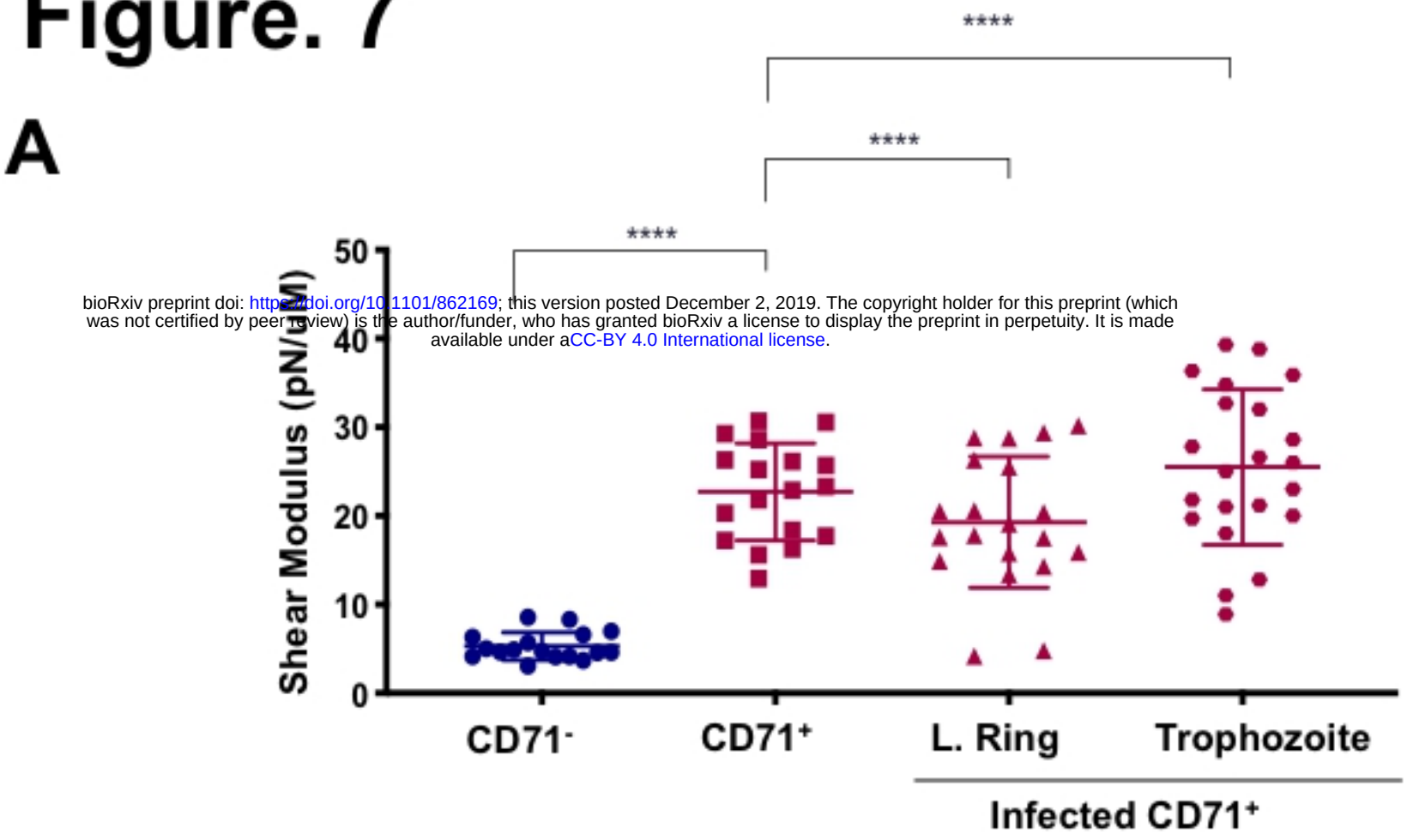

Figure. 7